

$U(1)_{B_3-L_2}$ Explanation of the Neutral Current B –Anomalies

B. C. Allanach¹

¹DAMTP, University of Cambridge, Wilberforce Road, Cambridge, CB3 0WA, United Kingdom

Received: date / Accepted: date

Abstract We investigate a speculative short-distance force, proposed to explain discrepancies observed between measurements of certain neutral current decays of B hadrons and their Standard Model predictions. The force derives from a spontaneously broken, gauged $U(1)_{B_3-L_2}$ extension to the Standard Model, where the extra quantum numbers of Standard Model fields are given by third family baryon number minus second family lepton number. The only fields beyond those of the Standard Model are three right-handed neutrinos, a gauge field associated with $U(1)_{B_3-L_2}$ and a Standard Model singlet complex scalar which breaks $U(1)_{B_3-L_2}$, a ‘flavon’. This simple model, via interactions involving a TeV scale force-carrying Z' vector boson, can successfully explain the neutral current B –anomalies whilst accommodating other empirical constraints. In an ansatz for fermion mixing, a combination of up-to-date B –anomaly fits, LHC direct Z' search limits and other bounds rule out the domain $0.15 \text{ TeV} < M_{Z'} < 1.9 \text{ TeV}$ at the 95% confidence level. For more massive Z' s, the model possesses a *flavonstrahlung* signal, where pp collisions produce a Z' and a flavon, which subsequently decays into two Higgs bosons.

1 Introduction

Data from the first decade of running of Large Hadron Collider (LHC) experiments involving the decays of B hadrons show some discrepancies with Standard Model (SM) predictions. For example, measurements of the ratio of branching ratios $R_{K^{(*)}} = BR(B \rightarrow K^{(*)} \mu^+ \mu^-) / BR(B \rightarrow K^{(*)} e^+ e^-)$ [1,2], $BR(B_s \rightarrow \mu^+ \mu^-)$ [3,4,5,6] and some angular distributions in $K^* \mu^+ \mu^-$ decays [7,8,9,10,11,12] all show some discrepancy (there are others). Each

discrepant observable is only 1-4 σ away from SM predictions but collectively, they point to a roughly similar conclusion. Despite a recent flagship LHCb measurement of R_K fluctuating somewhat toward its SM prediction (announced at the Moriond 2019 conference), the overall picture remains. Relative theoretical uncertainties, while taken into account in the number of sigma, vary from less than 1% to 20%, depending on the particular observable in question. In summary, several measurements of B hadron decays are somewhat inconsistent with the SM prediction of the $(\bar{s}b)(\bar{\mu}\mu)$ effective coupling. We call these discrepancies the neutral current¹ B –anomalies (NCBAs).

Several different fits to over a hundred B –observables [14, 15, 16, 17, 18, 19, 20] broadly agree: they favour a beyond the SM contribution to the weak effective theory operator

$$\mathcal{L}_{BSM} = -C_9 \mathcal{N}(\bar{s}\gamma^\rho P_L b)(\bar{\mu}\gamma_\rho \mu) + H.c., \quad (1)$$

where $\mathcal{N} = 1/(36 \text{ TeV})^2$ (in the present paper, $C_9 \neq 0$ means a contribution *beyond* the SM). We shall focus on one of the fits for definiteness: Ref. [17], where the result is that

$$C_9 = -0.97 \pm 0.15. \quad (2)$$

The coefficient of the operator at the best-fit point has a pull of 5.9 σ away from the SM value of 0 (taking the operator with P_L inserted before the final μ field in (1) provides an even better, but comparable, fit, 6.6 σ away from the SM value).

One possibility to generate such beyond the SM contributions is from the interactions of a new electrically neutral, massive, force carrying particle, dubbed a Z' ,

¹This is to distinguish some other discrepancies in $BR(B \rightarrow D^{(*)} \tau \nu) / BR(B \rightarrow D^{(*)} l \nu)$ [13], which are charged current processes and which we do not address.

^ae-mail: B.C.Allanach@damtp.cam.ac.uk

which has family dependent interactions. In particular, in order to explain the B -anomalies, the Lagrangian density should include (with the possible inclusion or exclusion of the second term) the interaction terms

$$\mathcal{L}_{int} = -g_{\mu_L} \overline{\mu_L} \not{Z}' \mu_L - g_{\mu_R} \overline{\mu_R} \not{Z}' \mu_R - g_{sb} \left(\overline{s_L} \not{Z}' b_L + H.c. \right), \quad (3)$$

where g_{sb} , g_{μ_L} and g_{μ_R} are all dimensionless coupling constants. Once the Z' is integrated out, in the weak effective field theory, one obtains the Lagrangian density terms

$$\mathcal{L}_{WET} = -\frac{g_{sb} g_{\mu_L}}{M_{Z'}^2} (\overline{s_L} \gamma^\rho b_L) (\overline{\mu_L} \gamma_\rho \mu_L) - \frac{g_{sb} g_{\mu_R}}{M_{Z'}^2} (\overline{s_L} \gamma^\rho b_L) (\overline{\mu_R} \gamma_\rho \mu_R) + H.c. \quad (4)$$

These are precisely of the type that can explain the NCBA: identifying (1) and (4) we see that

$$C_9 = g_{sb} (g_{\mu_L} + g_{\mu_R}) (36 \text{ TeV} / M_{Z'})^2. \quad (5)$$

Many models of flavoured Z' vector bosons have been invented based on spontaneously broken gauged $U(1)$ flavour symmetries [21, 22], for example from $L_\mu - L_\tau$ and other groups [23, 24, 25, 26, 27, 28, 29, 30, 31, 32, 33, 34, 35, 36, 37, 38, 39, 40, 41, 42, 43, 44, 45, 46, 21, 47, 48, 49, 50, 51, 52, 53, 54, 55, 56, 57, 58, 59]. Some models have several abelian groups in the extension [60], whilst some others [61, 62, 63] generate beyond the SM contributions with loop-level penguin diagrams. Some of the models are more ambitious than others, providing more or less detail toward ultra-violet completion.

In Refs. [43, 45] a gauged $U(1)_{B_3-L_2}$ symmetry was proposed to explain the neutral current B -anomalies. Both papers are quite detailed in their exposition, providing information about fermion mass model building through additional vector-like representations of the gauge group.

In ref. [43], Alonso *et al* introduce three additional SM-singlet scalar fields charged under $U(1)_{B_3-L_3}$ and² a vector-like fermion for each Weyl fermion of the SM (plus three right-handed neutrinos). It was shown how all SM fermion masses and mixings can originate via the Froggatt-Nielsen mechanism [64]. The Froggatt-Nielsen mechanism derives effective SM Yukawa couplings from renormalisable interactions which appear to be non-renormalisable from the low energy effective field theory point of view, once some heavy particles (the additional heavy vector-like fermions) are integrated out of the theory. It was shown by Alonso *et al* how assumptions about hierarchies in their masses and further assumptions regarding the renormalisable couplings of

² $U(1)_{B_3-L_3}$ in the model is equivalent to $U(1)_{B_3-L_2}$ after a change of basis of leptonic fields.

the model translate into empirically feasible values of fermion masses and fermion mixing.

In Ref. [45], Bonilla *et al* introduce two SM-singlet scalars that are charged under $U(1)_{B_3-L_2}$ along with a second Higgs doublet, also charged under $U(1)_{B_3-L_2}$. Two vector-like quark doublet representations are included. Once these scalar fields acquire vacuum expectation values (with various hierarchies between them assumed), a realistic pattern of neutrino masses and mixing can be achieved. In this model, Yukawa couplings leading to quark mixing are obtained already at the renormalisable level, without invoking the Froggatt-Nielsen mechanism.

The most robustly testable part of the phenomenology of the models of Alonso *et al* and Bonilla *et al* is that of the Z' , since it is the interactions of the Z' that explain the NCBA. Since the Z' contributes to processes other than those included in the NCBA, compatibility with measurements of these other processes then provides constraints upon each model. In both analyses, contributions from the additional non- Z' states to the NCBA and to other constraints were neglected by choosing parameters such that the additional states decouple.

It is our purpose here to examine the up-to-date collider phenomenology of similar models without worrying about the details of the physics that fixes the fermion mass data. To this end, we provide a simplified broad-brush formulation of a low energy effective field theory of a gauged, spontaneously broken $U(1)_{B_3-L_2}$ model and apply the latest bounds and fits, which have changed since the original analyses of Refs. [43, 45] due to a significantly increased integrated luminosity at the LHC. Since the original analyses, Z' constraints from direct searches have had an increase from 36 fb^{-1} to 139 fb^{-1} and the NCBA fits have changed due to the inclusion of further B meson decay data in some of the observables (the LHCb data set roughly doubling in size). In the effective field theory, we shall include the Z' boson as well as the flavon, a complex scalar field whose vacuum expectation value breaks $U(1)_{B_3-L_2}$. We shall neglect to specify other fields of the model, arguing that (along similar lines to Alonso *et al* and Bonilla *et al*) our analysis should capture the most pertinent features of the most currently relevant phenomenology, provided other states are sequestered from it either by sufficiently weak couplings or heavy masses. Thus, compared to Refs. [43, 45], we do not have as detailed a model of fermion masses but instead we have, in the back of our minds (such as through the Froggatt-Nielsen mechanism or through mixing with heavy vector-like fermion representations) an idea of how some small perturbations may be generated to correct the textures of Yukawa

Q'_{Li}	u'_{Ri}	d'_{Ri}	L'_1	L'_2	L'_3
0	0	0	0	-3	0
e'_{R1}	e'_{R2}	e'_{R3}	ν'_{R1}	ν'_{R2}	ν'_{R3}
0	-3	0	0	-3	0
Q'_{L3}	u'_{R3}	d'_{R3}	H	θ	
1	1	1	0	q_θ	

Table 1 $B_3 - L_2$ charge assignments of fields. A prime denotes a weak eigenstate Weyl fermion. Under $SU(3) \times SU(2)_L \times U(1)_Y$, the fields have representation $Q'_{Lj} \sim (3, 2, 1/6)$, $L'_{Lj} \sim (1, 2, -1/2)$, $e'_{Rj} \sim (1, 1, -1)$, $d'_{Rj} \sim (3, 1, -1/3)$, $u'_{Rj} \sim (3, 1, 2/3)$, $\nu'_{Rj} \sim (1, 1, 0)$, $H = (H^+, H^0)^T \sim (1, 2, 1/2)$, respectively. $i \in \{1, 2\}$, $j \in \{1, 2, 3\}$ are family indices. The flavon, θ , is a SM-singlet complex scalar field and q_θ is a non-zero rational real number.

matrices that are predicted at the level of the renormalisable, unbroken $U(1)_{B_3-L_2}$ theory. However, the latest bounds and fits presented here will be applicable to all models where assumptions about the flavour mixing of the Z' couplings match ours and where other states are sufficiently decoupled.

Our paper proceeds as follows: in §2, we define the effective $U(1)_{B_3-L_2}$ model, examining the Z' couplings to fermions, which are of paramount importance for phenomenology. To specify a model for phenomenological study, it is necessary to make further assumptions about fermion mixing; these are made in §3. Then, in §4, we examine the current consistency of NCBA fits with the other experimental constraints. A novel signal process, *flavonstrahlung*, is identified. In §5, we provide a summary and discussion. Technical definitions of mixing matrices and fields are made available in Appendix A.

2 $B_3 - L_2$ Model

The gauge group of the model is $SU(3) \times SU(2)_L \times U(1)_Y \times U(1)_{B_3-L_2}$. We display the charge assignments of the fields in the model under $U(1)_{B_3-L_2}$ in Table 1. The chiral fermions are all in *vector-like* representations with respect to $U(1)_{B_3-L_2}$ and so standard arguments imply that the symmetry is free from local perturbative anomalies, given that the SM plus three right-handed neutrinos is already free of local gauge anomalies under $SU(3) \times SU(2)_L \times U(1)_Y$.

At the renormalisable unbroken level, $U(1)_{B_3-L_2}$ predicts that the Yukawa matrices of SM fermions (see Appendix A for definitions and conventions) have the texture

$$Y_u \sim \begin{pmatrix} \times & \times & 0 \\ \times & \times & 0 \\ 0 & 0 & \times \end{pmatrix}, Y_d \sim \begin{pmatrix} \times & \times & 0 \\ \times & \times & 0 \\ 0 & 0 & \times \end{pmatrix}, Y_e \sim \begin{pmatrix} \times & 0 & \times \\ 0 & \times & 0 \\ \times & 0 & \times \end{pmatrix}, \quad (6)$$

where \times denotes an arbitrary dimensionless entry, which may be non-zero. From this prediction, we deduce that the Cabibbo-Kobayashi-Maskawa (CKM) matrix has zero entries for V_{ub} , V_{cb} , V_{ts} and V_{td} . However, the $U(1)_{B_3-L_2}$ symmetry is spontaneously broken by the vacuum expectation value $\langle \theta \rangle$ of a flavon: a SM singlet scalar θ with non-zero $B_3 - L_2$ charge q_θ . This breaking will replace the zero entries in (6) by small corrections generated by non-renormalisable operators. The model then predicts that the magnitudes of the CKM matrix entries V_{ub} , V_{cb} , V_{ts} and V_{td} are suppressed from unity by some small factor. This qualitative expectation [43, 45] agrees with current experimental estimates: $|V_{cb}| = (41.0 \pm 1.4) \times 10^{-3}$, $|V_{ub}| = (3.82 \pm 0.24) \times 10^{-3}$, $|V_{td}| = (8.0 \pm 0.3) \times 10^{-3}$, $|V_{ts}| = (38.8 \pm 1.1) \times 10^{-3}$ [13]. We note that fermion mass data dictate that there should be hierarchies within the \times symbols of each matrix in (6). A more complete ultra-violet theory could explain such hierarchies. The (33) entry of each matrix should *not* be suppressed, in order to explain the hierarchically large masses of third family fermions as compared to the other two families. Smaller corrections to the zeroes will then indeed predict small entries for the magnitudes of V_{ub} , V_{cb} , V_{ts} and V_{td} .

Neutrinos acquire mass through the see-saw mechanism with an initial symmetric mass matrix (whose basis is defined in (A.4)):

$$M_\nu = \begin{pmatrix} 0 & 0 & 0 & \dagger & 0 & \dagger \\ 0 & 0 & 0 & 0 & \dagger & 0 \\ 0 & 0 & 0 & \dagger & 0 & \dagger \\ \dagger & 0 & \dagger & * & 0 & * \\ 0 & \dagger & 0 & 0 & 0 & 0 \\ \dagger & 0 & \dagger & * & 0 & * \end{pmatrix}, \quad (7)$$

where the entries marked \dagger are of order the electroweak scale multiplied by the neutrino Yukawa couplings Y_ν and we expect the entries marked $*$ to be much greater than \dagger , since the mass scale $*$ is not fixed to the electroweak scale by any symmetry. As it stands, (7) has two eigenvalues of order $*$, two of order \dagger and two of order $\dagger^2/*$. However, we expect some of the zeroes in (7) to be corrected by ‘small’ non-renormalisable corrections from the spontaneous breaking of $U(1)_{B_3-L_2}$: in particular, the bottom right-hand 3 by 3 sub-matrix will be corrected by terms of order $*$ times a small number. It is expected that such corrections will still be many orders of magnitude above \dagger . Depending on the value of q_θ , some of the other entries may be corrected by terms of order $\langle \theta \rangle$. However, it is not our intention here to go into the minutæ of fermion mass model building for the model; instead we shall be content with the ‘broad-brush’ sketch expected of three very light neutrinos and three very heavy ones resulting from the expected small corrections and the see-saw mechanism.

We begin with the couplings of the $U(1)_{B_3-L_2}$ gauge boson Z'_μ to fermions in the Lagrangian in the weak (primed) eigenbasis

$$\mathcal{L}_{Z'\psi} = -g_{Z'} \left(\overline{Q'_{3L}} \not{Z}' Q'_{3L} + \overline{u'_{3R}} \not{Z}' u'_{3R} + \overline{d'_{3R}} \not{Z}' d'_{3R} - 3\overline{L'_{2L}} \not{Z}' L'_{2L} - 3\overline{e'_{2R}} \not{Z}' e'_{2R} - 3\overline{\nu'_{2R}} \not{Z}' \nu'_{2R} \right), \quad (8)$$

where $g'_{Z'}$ is the $U(1)_{B_3-L_2}$ gauge coupling. $U(1)_{B_3-L_2}$ is broken by $\langle \theta \rangle \neq 0$ and so the Z' acquires a mass

$$M_{Z'} = q\theta g_F \langle \theta \rangle. \quad (9)$$

We shall see below that a combination of LHC search bounds and NCBAAs will imply that $M_{Z'}$ is at least of order the TeV scale. We assume that the approximately right-handed neutrinos discussed above have a much higher mass than $M_{Z'}$. The Z' boson ‘eats’ one real degree of freedom of θ via the Brout-Englert-Higgs mechanism [65,66] to form its longitudinal polarisation mode. In the spontaneously broken theory, we expand $\theta = (\langle \theta \rangle + \vartheta)/\sqrt{2}$, in terms of the one real physical flavon degree of freedom, ϑ . Its tree-level mass m_ϑ , depends on free parameters in the θ potential, but barring special circumstances we may expect it to be of order $\langle \theta \rangle$.

Writing the weak eigenbasis fermionic fields as 3-dimensional vectors in family space $\mathbf{u}_R', \mathbf{Q}_L' = (\mathbf{u}_L', \mathbf{d}_L')$, $\mathbf{e}_R', \mathbf{d}_R', \mathbf{L}_L' = (\nu_L', \mathbf{e}_L')$, we define the 3 by 3 unitary matrices V_P , where $P \in \{u_R, d_L, u_L, e_R, u_R, d_R, \nu_L, e_L\}$. V_{d_L} transform between the weak eigenbasis and the mass (unprimed) eigenbasis³ as detailed in Appendix A:

$$\mathbf{P}' = V_P \mathbf{P}. \quad (10)$$

Re-writing (8) in the mass eigenbasis and using the quark and lepton mixing matrices V and U defined in (A.8)

$$\begin{aligned} \mathcal{L}_{Z'\psi} = & -g_{Z'} \left(\overline{\mathbf{d}_L} \Lambda_\Xi^{(d_L)} \not{Z}' \mathbf{d}_L + \overline{\mathbf{u}_L} \Lambda_\Xi^{(u_L)} \not{Z}' \mathbf{u}_L \right. \\ & + \overline{\mathbf{u}_R} \Lambda_\Xi^{(u_R)} \not{Z}' \mathbf{u}_R + \overline{\mathbf{d}_R} \Lambda_\Xi^{(d_R)} \not{Z}' \mathbf{d}_R \\ & - 3\overline{\mathbf{e}_L} \Lambda_\Omega^{(e_L)} \not{Z}' \mathbf{e}_L - 3\overline{\nu_L} \Lambda_\Omega^{(\nu_L)} \not{Z}' \nu_L \\ & \left. - 3\overline{\mathbf{e}_R} \Lambda_\Omega^{(e_R)} \not{Z}' \mathbf{e}_R - 3\overline{\nu_R} \Lambda_\Omega^{(\nu_R)} \not{Z}' \nu_R \right). \quad (11) \end{aligned}$$

We have defined the 3 by 3 dimensionless Hermitian coupling matrices

$$\Lambda_\alpha^{(I)} := V_I^\dagger \alpha V_I, \quad (12)$$

where $I \in \{u_L, d_L, e_L, \nu_L, u_R, d_R, e_R, \nu_R\}$, $\alpha \in \{\Xi, \Omega\}$ and

$$\Xi := \begin{pmatrix} 0 & 0 & 0 \\ 0 & 0 & 0 \\ 0 & 0 & 1 \end{pmatrix}, \quad \Omega := \begin{pmatrix} 0 & 0 & 0 \\ 0 & 1 & 0 \\ 0 & 0 & 0 \end{pmatrix}. \quad (13)$$

³ \mathbf{P} and \mathbf{P}' are column vectors.

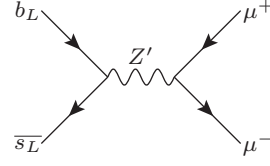


Fig. 1 Tree-level Feynman diagram of a process which contributes to the NCBAAs.

Provided that $(V_{d_L})_{23} \neq 0$, (11) contains tree-level couplings of the Z' to $\overline{b_L} s_L$, $\overline{s_L} b_L$ and $\mu^+ \mu^-$. Thus, it shows promise to explain the NCBAAs through processes such as the one in Fig. 1.

3 Example Case

In order to specify the model further, we should detail the mixing matrices V_I . However, we have not constructed a detailed model for them. Here, we shall make a simple ansatz for fermion mixing matrices which is likely to not be ruled out by other flavour bounds on flavour changing neutral currents but which is favourable from the point of view of the NCBAAs. For example, in order to successfully describe the NCBAAs, we require $(V_{d_L})_{23} \neq 0$. We shall examine the limit (which we call ‘ $(B_3 - L_2)\text{eg}$ ’) where

$$V_{d_L} = \begin{pmatrix} 1 & 0 & 0 \\ 0 \cos \theta_{sb} & -\sin \theta_{sb} \\ 0 \sin \theta_{sb} & \cos \theta_{sb} \end{pmatrix}, \quad (14)$$

$V_{d_R} = 1, V_{e_R} = 1, V_{e_L} = 1$ and $V_{u_R} = 1$, meaning that $V_{u_L} = V_{d_L} V^\dagger$, $V_{\nu_L} = U^\dagger$, where U is the lepton mixing matrix defined in Appendix A. Thus, the predicted tree-level flavour changing neutral currents are, aside from the Z' coupling to $\overline{b}s$ and $\overline{s}b$, relegated to the up quarks and neutrinos, where the bounds from experiment are significantly weaker. Our assumptions here are of course strong, but they merely constitute an example case for phenomenological study in order to assess viability. Extracting the couplings of the Z' relevant for the NCBAAs, we have

$$\mathcal{L} = -g_{Z'} \left[\left(\frac{1}{2} \sin 2\theta_{sb} \overline{s} \not{Z}' P_L b + H.c. \right) - 3\overline{\mu} \not{Z}' \mu \right] + \dots \quad (15)$$

Thus, by identifying (15) with (5), we have

$$g_{sb} = \frac{g_{Z'}}{2} \sin 2\theta_{sb}, \quad g_{\mu L} = g_{\mu R} = -\frac{3g_{Z'}}{2}. \quad (16)$$

4 Phenomenology

We have now specified the $(B_3 - L_2)\text{eg}$ enough to apply experimental constraints to it. We first bound its free parameters through the fit to the NCBAAs and then go on to derive other pertinent bounds before considering predictions.

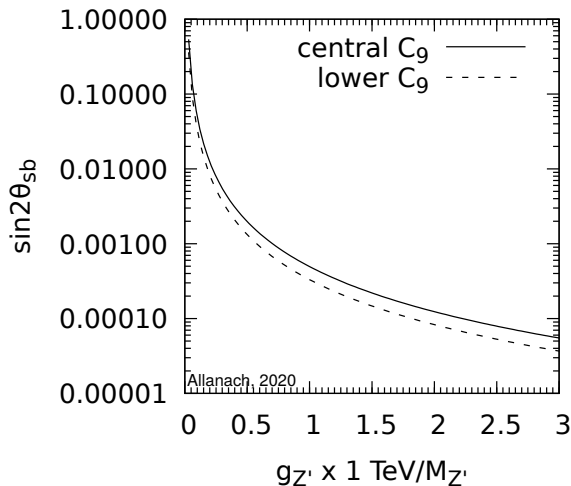


Fig. 2 $\sin 2\theta_{sb}$ in the $(B_3 - L_2)$ eg as constrained by a fit [17] to the NCBAAs in (18). Central $C_9 = -0.97$ and lower $C_9 = -0.65$.

4.1 Fit to NCBAAs

At energy scales far below $M_{Z'}$, in the effective theory where the Z' is integrated out, (15) becomes

$$\mathcal{L} = \frac{3g_{Z'}^2}{2M_{Z'}^2} \sin 2\theta_{sb} (\bar{s}\gamma^\rho P_L b)(\bar{\mu}\gamma_\rho \mu) + H.c., \quad (17)$$

where γ^ρ are Dirac matrices, P_L is a left-handed projection matrix and $\rho \in \{0, 1, 2, 3\}$ is a space-time index. The fits prefer no sizeable contributions from the operator obtained by switching $P_L \rightarrow P_R$ in (17) [17] and indeed, since we have assumed $V_{dR} = 1$, we predict none (at tree level). Substituting g_{sb} , $g_{\mu L}$ and $g_{\mu R}$ from (16) into (5), we have

$$\sin 2\theta_{sb} = -5.1 \times 10^{-4} \left(\frac{M_{Z'}}{g_{Z'} \text{TeV}} \right)^2 C_9. \quad (18)$$

Requiring that $\sin 2\theta_{sb} \leq 1$ implies that

$$g_{Z'} \frac{\text{TeV}}{M_{Z'}} \geq 0.023 \sqrt{C_9 / (-0.97)}. \quad (19)$$

The $(B_3 - L_2)$ eg has three pertinent free parameters: $M_{Z'}$, θ_{sb} and $g_{Z'}$. It will suit us to adopt (18) with the empirically-fitted input for C_9 in order to reduce the number of free-parameters to two, so that the parameter space of the model can be captured and plotted in two dimensions. The central value of C_9 as extracted from fits to the NCBAAs shown in (2) will be the ‘central C_9 ’ value of -0.97, however we will also refer to the ‘lower C_9 ’ value. This is the value of C_9 which is closest to the SM limit but still fits the relevant data to within 2σ (i.e. $C_9 = -0.65$ [17]). We display the value of $\sin 2\theta_{sb}$ for these two cases in Fig. 2.

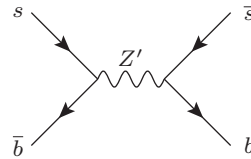


Fig. 3 Tree-level Feynman diagram of a beyond the SM contribution to $B_s - \bar{B}_s$ mixing.

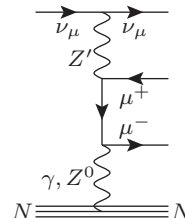


Fig. 4 Tree-level Feynman diagram of a beyond the SM contribution to the neutrino trident process.

4.2 $B_s - \bar{B}_s$ mixing

Since our Z' couples to bottom and strange (anti-)quarks, it induces a beyond the SM contribution to $B_s - \bar{B}_s$ mixing via the process in Fig. 3. The value of the bound depends on lattice data [67] which change the SM prediction. These have varied significantly over the last decade. We use a recent determination based on lattice data and sum rules [68] which implies that⁴ $g_{Z'} \sin 2\theta_{sb}/2 \leq M_{Z'}/194 \text{ TeV}$ [69]. Using (18), this implies the lower bound

$$g_{Z'} \frac{\text{TeV}}{M_{Z'}} \geq 0.048 \frac{C_9}{-0.97}. \quad (20)$$

The fact that this is a *lower* bound might at first seem counter-intuitive, until one realises that, for lower values of $g_{Z'} \text{TeV}/M_{Z'}$, one can only fit the NCBAAs with a larger value of $\sin 2\theta_{sb}$, i.e. a larger Z' coupling to bottom and strange (anti-)quarks and therefore a larger contribution to $B_s - \bar{B}_s$ mixing.

4.3 Neutrino trident

Z' 's which couple to muon neutrinos contribute to the process $\nu_\mu N \rightarrow \nu_\mu N \mu^+ \mu^-$, where N is a heavy nucleus, for example by the process depicted in Fig. 4 (there are other diagrams involving W bosons). In the heavy Z' limit, the predicted tree-level ratio of the $(B_3 - L_2)$ eg model cross-section to the SM one is [45]

$$\frac{\sigma_{(B_3 - L_2)\text{eg}}}{\sigma_{SM}} = \frac{1 + (1 + 4s_W^2 + 18v^2 g_{Z'}^2 / M_{Z'}^2)^2}{1 + (1 + 4s_W^2)^2}, \quad (21)$$

⁴In the present paper, we quote all single-sided empirical bounds at the 95% confidence level.

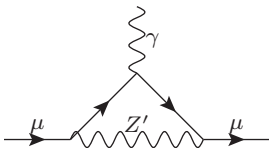


Fig. 5 Leading new physics contribution to the anomalous magnetic moment of the muon.

where v is the SM Higgs vacuum expectation value and s_W is the sine of the Weinberg angle. The measurement of the neutrino trident cross section by the CCFR collaboration yields the constraint $\sigma_{(B_3-L_2)\text{eg}}/\sigma_{SM} \leq 1.38$ [70]. Using the central values $v = 246.22$ GeV and $s_W^2 = 0.22337$ [13] in (21), this yields

$$g_{Z'} \frac{\text{TeV}}{M_{Z'}} \leq 0.62. \quad (22)$$

4.4 Anomalous Magnetic Moment of the Muon

The $U(1)_{B_3-L_2}\text{eg}$ has the potential to explain measurements of the anomalous magnetic moment of the muon $(g-2)_\mu$, which disagrees with SM predictions. Current estimates for the discrepancy are [13]

$$\Delta a_\mu = \frac{\Delta(g-2)_\mu}{2} = (26.1 \pm 6.3 \pm 4.8) \times 10^{-10}, \quad (23)$$

where the first uncertainty quoted is experimental and the second theoretical. Adding the uncertainties in quadrature implies that there is a 3.3σ discrepancy between SM predictions and the experimental measurement. A leading contribution to Δa_μ from the Z' is depicted in Fig. 5. In total, the Z' corrections yield [71]

$$\Delta a_\mu((B_3 - L_2)\text{eg}) = \frac{3g_{Z'}^2}{4\pi^2} \left[\frac{m_\mu^2}{M_{Z'}^2} + \mathcal{O}\left(\frac{m_\mu^4}{M_{Z'}^4}\right) \right]. \quad (24)$$

Equating (23),(24), we find that in order to fit the anomalous magnetic moment at the 2σ level,

$$1.1 < g_{Z'} \frac{\text{TeV}}{M_{Z'}} < 2.2. \quad (25)$$

Comparing with (22), we see that the 2σ region preferred by measurements of the anomalous magnetic moment of the muon are in tension with CCFR measurements of the neutrino trident process.

4.5 $Z^0 \rightarrow \mu^+ \mu^- Z'$

For Z' particles whose mass is less than that of the Z^0 boson, i.e. $M_{Z'} < M_Z$, a recent CMS search in 77.3 fb^{-1} of 13 TeV pp collisions for $Z^0 \rightarrow \mu^+ \mu^- Z'$ followed by $Z' \rightarrow \mu^+ \mu^-$ provides constraints [72]. Stringent 95% upper bounds upon the product of branching ratios

$$R_{4\mu} = BR(Z^0 \rightarrow \mu^+ \mu^- Z') \times BR(Z' \rightarrow \mu^+ \mu^-)$$

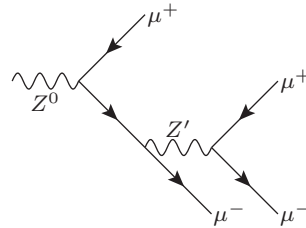


Fig. 6 Tree-level diagram of a new physics contribution to $Z \rightarrow 4\mu$ decay.

at the level of $10^{-7} - 10^{-8}$ are presented as a function of $M_{Z'} \in [5 \text{ GeV}, 70 \text{ GeV}]$. For a given value of $M_{Z'}$ in the aforementioned range and a reference value of $g_{Z'}$, we use `MadGraph_2_6_5` [73] to calculate the value of $R_{4\mu}$. In the parameter range considered for which this decay is relevant, $BR(Z' \rightarrow \mu^+ \mu^-)$ is independent of $g_{Z'}$ to a very good approximation and so $R_{4\mu}$ is predicted to be proportional to $g_{Z'}^2$. We can thus scale $g_{Z'}$ to find its value at the 95% upper limit.

4.6 Z' width and perturbativity

The partial width of a Z' decaying into a Weyl fermion f_i and Weyl anti-fermion \bar{f}_j is

$$\Gamma_{ij} = \frac{C}{24\pi} |g_{ij}|^2 M_{Z'}, \quad (26)$$

where g_{ij} is the coupling of the Z' boson to $f_i \bar{f}_j$ and C is the number of colour degrees of freedom of the fermions (here, 3 or 1). In the limit that $m_t/M_{Z'} \rightarrow 0$, we may approximate all fermions as being massless. Summing over fermion species (it is simplest to do this in the weak eigenbasis), we obtain a total width Γ :

$$\frac{\Gamma}{M_{Z'}} = \frac{13g_{Z'}^2}{8\pi}. \quad (27)$$

To remain in the perturbative régime such that we may trust our perturbative calculations, we should have $\Gamma/M_{Z'} < 1$, i.e. $g_{Z'} < \sqrt{8\pi/13} = 1.4$. Substituting this into (20) yields an upper bound $M_{Z'} \leq 29(-0.97/C_9)$ TeV from perturbativity, fits to NCBA and $B_s - \bar{B}_s$ mixing measurements.

4.7 LHC Z' Searches

The ATLAS experiment has performed various searches in pp collisions at the LHC for resonant Z' vector bosons decaying into different final states. None of them have found a significant signal to date and so lower limits are placed upon the production cross-sections times branching ratio as a function of the invariant mass of the final state. For example, a 36.1 fb^{-1} 13 TeV search

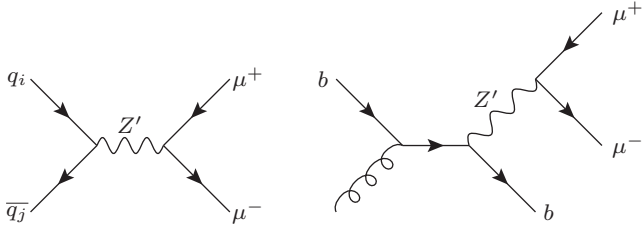


Fig. 7 Example Feynman diagrams of tree-level $B_3 - L_2$ inclusive Z' production at the LHC followed by decay into muons. $q_{i,j} \in \{u, c, d, s, b\}$ are such that the combination $q_i \bar{q}_j$ has zero electric charge.

in $t\bar{t}$ imposes $\sigma \times BR(Z' \rightarrow t\bar{t}) < 10$ fb for large $M_{Z'}$ [74, 75]. A di-tau final state search from the 8 TeV run imposes $\sigma \times BR(Z' \rightarrow \tau^+ \tau^-) < 3$ fb for large $M_{Z'}$ [76]. However, the most constraining channel to date for the $(B_3 - L_2)$ eg is from a $Z' \rightarrow \mu^+ \mu^-$ in 139 fb^{-1} of 13 TeV pp collisions [77], where, for $M_{Z'} = 6$ TeV, $\sigma \times BR(Z' \rightarrow \mu^+ \mu^-) < 0.015$ fb, where σ is the fiducial Z' production cross-section. We shall therefore use this search to constrain the model⁵. Feynman diagrams of example Z' production signal processes are shown in Fig. 7.

In this ATLAS di-muon resonance search, each muon is required to have a transverse momentum $p_T > 30$ GeV, pseudo-rapidity magnitude $|\eta| < 2.5$ and a di-muon invariant mass $m_{\mu\mu} > 225$ GeV. ATLAS has already taken efficiencies into account in their published bounds so there is no need to simulate the detector. Upper bounds $s(M_{Z'}, z)$ on $\sigma \times BR(Z' \rightarrow \mu^+ \mu^-)$ are published for $z := \Gamma/M_{Z'}$ values from 0 to 0.1 [78]. In Ref. [69], it was shown that a function

$$s(z, M_{Z'}) = s(0, M_{Z'}) \left[\frac{s(0.1, M_{Z'})}{s(0, M_{Z'})} \right]^{0.1} \quad (28)$$

fits the given published bounds well in the given domain $z \in [0, 0.1]$. We shall also use (28) to extrapolate slightly outside of this domain, but will delineate regions of parameter space where the bound is extrapolated rather than interpolated.

The $(B_3 - L_2)$ eg model was encoded into UFO format via `FeynRules` [79, 80] for inclusion into an event generator. We calculate the fiducial cross-section $\sigma(pp \rightarrow Z' \rightarrow \mu^+ \mu^-)$ with the `MadGraph_2_6_5` [73] event generator for a centre of mass energy of 13 TeV. We have added the possibility of producing an additional jet along with the Z' so that the second diagram of Fig. 7 is included in our estimate of the cross-section. We also use five flavour parton distribution functions to re-sum initial state b -quark logarithms [81] and neglect interference with SM backgrounds. We display an allowed parameter space point ($M_{Z'} = 3$ TeV, $g_{Z'} = 0.15$) in

⁵The analogous CMS search has yet to be published

$M_{Z'}$	3 TeV
$g_{Z'}$	0.15
$\sin 2\theta_{sb}$	0.20
Γ	35 GeV
$s(M_{Z'}, z)$	0.069 fb
$\sigma(pp \rightarrow Z' \rightarrow \mu^+ \mu^-) (+j)$	0.033 fb
$BR(Z' \rightarrow \mu^+ \mu^-)$	0.46
$BR(Z' \rightarrow t\bar{t})$	0.15
$BR(Z' \rightarrow b\bar{b})$	0.15
$\sigma(b\bar{b} \rightarrow Z' \rightarrow \mu^+ \mu^-)$	0.026 fb
$\sigma(gb \rightarrow Z'b \rightarrow \mu^+ \mu^- b)$	0.007 fb
$\sigma(s\bar{b} \rightarrow Z' \rightarrow \mu^+ \mu^-)$	6.1×10^{-4} fb

Table 2 Example point in $(B_3 - L_2)$ eg parameter space that fits the NBCAs (for central $C_9 = -0.97$) and survives all constraints. We show the largest partonic contributions to the cross-section at the bottom of the table. For the last two rows, the CP conjugated process has been added to the cross-section contribution. ‘(+j)’ refers to the fact that the cross-section includes the addition of another jet in the final state.

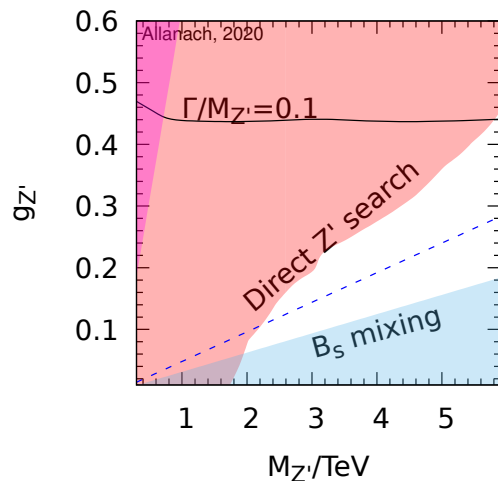


Fig. 8 Constraints upon $(B_3 - L_2)$ eg for $M_{Z'} > 300$ GeV. $\sin 2\theta_{sb}$ has been set as in (18) such that every point fits the NBCAs. The white region is currently allowed. The red and blue coloured regions show the 95% excluded regions from a 13 TeV 139 fb^{-1} ATLAS $Z' \rightarrow \mu^+ \mu^-$ search [77] and from $B_s - \bar{B}_s$ mixing as in (20), respectively. The latter bound moves from the blue coloured region at lower $C_9 = -0.65$ to the region below the dashed line for central $C_9 = -0.97$. The magenta region in the top left-hand corner shows the region ruled out by the neutrino trident process. The direct search bound is extrapolated above the solid curve and interpolated between ATLAS data below it, according to (28).

Table 2. From the table, we can see that the dominant process is $b\bar{b} \rightarrow Z' \rightarrow \mu^+ \mu^-$, the sub-dominant process is $(bg \rightarrow Z'b \rightarrow \mu^+ \mu^- b$ plus the CP conjugated process). The other tree-level processes simulated make a negligible contribution to the cross-section.

In Fig. 8, we display constraints upon the $(B_3 - L_2)_{\text{eg}}$ parameter space for $M_{Z'} > 300$ GeV. There is only a small region of parameter space where the ATLAS di-muon resonance search bounds have been extrapolated (slightly): above the solid curve. The white region of the figure is allowed by all constraints. We see that $M_{Z'} > 1.9$ TeV from these. The direct search constraint does not change by eye from the one shown in the figure when one chooses the central value of $C_9 = -0.97$ from the NCBA fit or the lower value. We may understand this by the fact that $\sin 2\theta_{sb}$ is small throughout the vast majority of the plot, whichever value of C_9 is used, in accordance with Fig. 2. The dominant Z' production amplitude is proportional to the $Z'\bar{b}b$ coupling, which is proportional to $g_{Z'} \cos 2\theta_{sb} \approx g_{Z'}$ and so loses the sensitivity⁶ that $\sin 2\theta_{sb}$ has on C_9 through (18). The B_s mixing bound is however sensitive to a change in C_9 (via its effect on g_{sb}) and the bound becomes the dashed line for central C_9 . So: for central C_9 , one concludes that $M_{Z'} > 2.2$ TeV. For either value of C_9 and throughout the allowed parameter space shown, $BR(Z' \rightarrow \mu^+\mu^-)$, $BR(Z' \rightarrow \bar{b}b)$ and $BR(Z' \rightarrow \bar{t}t)$ do not change (to the significant figure quoted) from the values in Table 2.

Bonilla *et al* showed that, in the model of Ref. [45], a region of parameter space with $M_{Z'} < 300$ GeV could pass all constraints. We now re-examine this lighter mass range; our analysis closely follows that of Bonilla *et al*, except for the fact that we constrain the parameter space to always fit the NCBA and that we have updated the constraints from $Z \rightarrow \mu^+\mu^- Z' \rightarrow 4\mu$ with a new search from CMS.

The ATLAS search for $Z' \rightarrow \mu^+\mu^-$ used above provided no constraints for $M_{Z'} \leq 300$ GeV. Thus, we have used an earlier ATLAS search⁷ for $Z' \rightarrow \mu^+\mu^-$ in 36.1^{-1} fb of 13 TeV pp collisions, which presented exclusions on generic⁸ Z' 's for $M_{Z'} \geq 150$ GeV [82]. We calculate the acceptance (for muon transverse momenta $p_T > 30$ GeV and muon pseudorapidities $|\eta| < 2.5$) times cross section times branching ratio for $Z' \rightarrow \mu^+\mu^- (+j)$ using `MadGraph_2.6.5`. We find that the region $150 \text{ GeV} < M_{Z'} < 300 \text{ GeV}$ is excluded by this search for the entire domain $0.001 \leq g_{Z'} \leq 0.2$. The available parameter space is shown in Fig. 9. We see that the $(B_3 - L_2)_{\text{eg}}$ may fit the NCBA for $M_{Z'} < 150$ GeV while still passing other experimental constraints.

⁶(26) and (27) show that $BR(Z' \rightarrow \mu^+\mu^-)$ has no dependence on C_9 through $\sin 2\theta_{sb}$ either.

⁷A similar CMS search exists [72], but doesn't reach quite as low values of $M_{Z'}$ and so we do not use it.

⁸Since in the relevant part of the parameter space, our Z' 's are predicted to be very narrow, we use the bounds for the narrowest Z' 's given, i.e. $\Gamma_{Z'}/M_{Z'} = 0.02$.

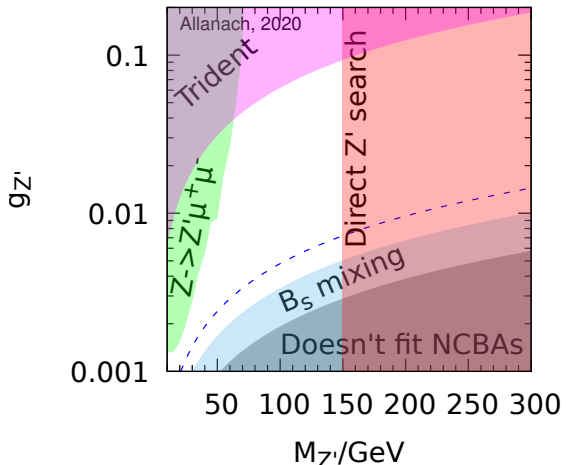


Fig. 9 Constraints upon $(B_3 - L_2)_{\text{eg}}$ for $M_{Z'} \leq 300$ GeV. $\sin 2\theta_{sb}$ has been set as in (18) such that every point fits the NCBA. The white region is currently allowed. The red and blue coloured regions show the 95% excluded regions from a 13 TeV 36.1 fb^{-1} ATLAS $Z' \rightarrow \mu^+\mu^-$ search [77] and from $B_s - \bar{B}_s$ mixing as in (20), respectively. The latter bound moves from the blue coloured region at lower $C_9 = -0.65$ to the region below the dashed line for central $C_9 = -0.97$. The magenta region shows the region ruled out by the neutrino trident process and the green region by a CMS search in 77.3 fb^{-1} of 13 TeV pp collisions for $Z^0 \rightarrow \mu^+\mu^- Z' \rightarrow 4\mu$ [72]. In the grey region at the bottom of the plot, the effect of the Z' on the NCBA is too weak to fit them.

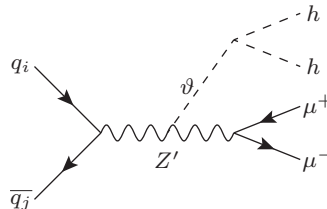


Fig. 10 Feynman diagram of *flavonstrahlung* process at a hadron collider. $q_{i,j} \in \{u, c, d, s, b\}$ are such that the combination $q_i \bar{q}_j$ has zero electric charge.

4.8 Flavonstrahlung

In the unbroken $U(1)_{B_3-L_2}$ theory, θ interacts with the Higgs boson via the Lagrangian density term $-\lambda_{\theta H} \theta \theta^\dagger H H^\dagger$. Supposing that the dimensionless coefficient $\lambda_{\theta H} \neq 0$, the flavon θ will then decay into two physical Higgs bosons hh with approximately 100% branching ratio. Moreover, the θ kinetic term leads to the Lagrangian density term $g_{Z'}^2 q_\theta^2 Z'_\mu Z'^{\mu} \langle \theta \rangle \theta$ after spontaneous symmetry breaking. Thus, if a proton-proton collider has sufficient energy and luminosity, it may produce $Z'\theta$, leading to the spectacular signature of $\mu^+\mu^- hh$, where $\mu^+\mu^-$ have a resonance at an invariant mass of $M_{Z'}$ and hh have one at the flavon mass m_θ . This ‘flavonstrahlung’ process is depicted in Fig. 10. Flavonstrahlung

would probably not be the first detection of beyond the SM physics in the model: Z' production followed by decay into $\mu^+\mu^-$ would most likely be the first, followed perhaps by $Z' \rightarrow t\bar{t}$ and $b\bar{b}$. Flavonstrahlung is suppressed compared to exclusive Z' production because of its larger final-state phase space and kinematics, and would thus require significantly more luminosity and partonic energy to detect.

5 Discussion

Spontaneously broken $U(1)_{B_3-L_2}$ [43,45] has parameter space that is consistent with contemporary direct search limits whilst fitting neutral current B -anomalies and passing other indirect bounds (the most constraining being those from measurements of $B_s - \bar{B}_s$ mixing).

We have provided a simple broad-brush formulation of the $U(1)_{B_3-L_2}$ model, similar to the one of the Third Family Hypercharge Model (TFHM) [54] and variants [83]. We then presented an example case for phenomenological study, the ‘ $(B_3 - L_2)\text{eg}$ ’. Fig. 8 shows that in the $(B_2 - L_2)\text{eg}$ the current empirical constraints imply that $M_{Z'} > 1.9$ TeV or $M_{Z'} < 150$ GeV. In the latter lighter region, one may obtain significant corrections to the anomalous magnetic moment of the muon (however, neutrino trident constraints are in 2σ tension with the current 2σ -preferred region of $(g - 2)_\mu$). The fact that $M_{Z'} < 150$ GeV is currently allowed motivates further effort in order to push interpretations of LHC $\mu^+\mu^-$ resonance searches to lower invariant masses where, admittedly, backgrounds are steeply increasing.

The constraints in Figs. 8,9 apply to any gauged, spontaneously broken $U(1)_{B_3-L_2}$ model where our assumptions about the Z' couplings detailed in §3 approximately hold. This is the case for the model of Alonso *et al* [43], which found the weaker bound of $M_{Z'} > 1.0$ TeV from the various predecessor constraint data and NCBA fits. The bound has moved to $M_{Z'} > 1.9$ TeV with the latest fits and data. Alonso *et al* did not consider $M_{Z'} < 300$ GeV, but our results in Fig. 9 show that $M_{Z'} < 150$ GeV is currently viable. The model of Bonilla *et al* [45] does not match the pattern of $(B_3 - L_2)\text{eg}$ Z' couplings to left-handed down quarks and so our results are not directly applicable to it.

The direct $Z' \rightarrow \mu^+\mu^-$ search constraints on the $(B_3 - L_2)\text{eg}$ in Fig. 8 are comparable to those on similarly constructed TFHMeg models⁹. In TFHMs though, the Higgs doublet is necessarily charged under the additional $U(1)$ in order to allow a renormalisable top

⁹In Refs. [54,83], the associated production process $Z'j$ was not included, however.

Yukawa coupling (which seems necessary, given that it is of order 1 and so is inconsistent with a small effective coupling induced by symmetry breaking). This leads to tree-level $Z - Z'$ mixing, associated strong bounds from inferences of the ρ parameter [84]: indeed, these entirely disallow the $M_{Z'} \leq 300$ GeV region for the TFHMs. The $U(1)_{B_3-L_2}$ model is not subject to these strong bounds, however, since the SM Higgs doublet is uncharged under $U(1)_{B_3-L_2}$.

In §4.8, we have identified a novel flavonstrahlung signal process, where pp collisions result in Z' plus flavon production, followed by Z' decay into $\mu^+\mu^-$ and flavon decay into hh . This process will also be present in other similar NCBA-explaining $U(1)$ extensions which are broken by a SM singlet, since the flavon field used to break the $U(1)$ extension will generically have couplings with the SM Higgs doublet. Thus, for example, TFHMs also predict the possibility of flavonstrahlung.

Acknowledgements

This work has been partially supported by STFC Consolidated HEP grants ST/P000681/1 and ST/T000694/1. We thank other members of the Cambridge Pheno Working Group and W. Murray for discussions.

Appendix A: Conventions and fermion mixing

Here, we detail the rotation of fermion fields to the mass basis in order to fix our conventions. We write

$$\begin{aligned} \mathbf{u}'_{\mathbf{L}} &= \begin{pmatrix} u'_L \\ c'_L \\ t'_L \end{pmatrix}, & \mathbf{d}'_{\mathbf{L}} &= \begin{pmatrix} d'_L \\ s'_L \\ b'_L \end{pmatrix}, & \boldsymbol{\nu}'_{\mathbf{L}} &= \begin{pmatrix} \nu'_{eL} \\ \nu'_{\mu L} \\ \nu'_{\tau L} \end{pmatrix}, \\ \mathbf{e}'_{\mathbf{L}} &= \begin{pmatrix} e'_L \\ \mu'_L \\ \tau'_L \end{pmatrix}, & \mathbf{u}'_{\mathbf{R}} &= \begin{pmatrix} u'_R \\ c'_R \\ t'_R \end{pmatrix}, & \mathbf{d}'_{\mathbf{R}} &= \begin{pmatrix} d'_R \\ s'_R \\ b'_R \end{pmatrix}, \\ \mathbf{e}'_{\mathbf{R}} &= \begin{pmatrix} e'_R \\ \mu'_R \\ \tau'_R \end{pmatrix}, & \boldsymbol{\nu}'_{\mathbf{R}} &= \begin{pmatrix} \nu'_{eR} \\ \nu'_{\mu R} \\ \nu'_{\tau R} \end{pmatrix}, \end{aligned} \quad (\text{A.1})$$

along with the SM fermionic electroweak doublets

$$\mathbf{Q}'_{\mathbf{L}i} = \begin{pmatrix} \mathbf{u}'_{\mathbf{L}i} \\ \mathbf{d}'_{\mathbf{L}i} \end{pmatrix}, \quad \mathbf{L}'_{\mathbf{L}i} = \begin{pmatrix} \nu'_{\mathbf{L}i} \\ \mathbf{e}'_{\mathbf{L}i} \end{pmatrix}. \quad (\text{A.2})$$

The fermions acquire their masses through the terms

$$-\mathcal{L}_Y = \overline{\mathbf{Q}'_{\mathbf{L}}}_u Y_u \tilde{H} \mathbf{u}'_{\mathbf{R}} + \overline{\mathbf{Q}'_{\mathbf{L}}}_d Y_d H \mathbf{d}'_{\mathbf{R}} + \overline{\mathbf{L}'_{\mathbf{L}}} Y_e H \mathbf{e}'_{\mathbf{R}} + \overline{\mathbf{L}'_{\mathbf{L}}} Y_\nu \tilde{H} \boldsymbol{\nu}'_{\mathbf{R}} + H.c. + \frac{1}{2} \overline{\boldsymbol{\nu}'_{\mathbf{R}}} M \boldsymbol{\nu}'_{\mathbf{R}}, \quad (\text{A.3})$$

where Y_u , Y_d and Y_e are dimensionless complex coupling constants, each written as a 3 by 3 matrix in family space. The matrix M is a 3 by 3 complex symmetric matrix of mass dimension 1, c denotes the charge

conjugate of a field and $\tilde{H} = (H^{0*}, -H^-)^T$. After electroweak symmetry breaking and the W^\pm boson eating the electrically charged components of the Higgs doublet, we may write $H = (0, (v+h)/\sqrt{2})$, where h is the physical Higgs boson field and (A.3) includes the fermion mass terms

$$\begin{aligned}
-\mathcal{L}_Y = & \overline{\mathbf{u}}'_L V_{uL} V_{uL}^\dagger m_u V_{uR} V_{uR}^\dagger \mathbf{u}'_R + \\
& \overline{\mathbf{d}}'_L V_{dL} V_{dL}^\dagger m_d V_{dR} V_{dR}^\dagger \mathbf{d}'_R + \\
& \overline{\mathbf{e}}'_L V_{eL} V_{eL}^\dagger m_e V_{eR} V_{eR}^\dagger \mathbf{e}'_R + \\
& \frac{1}{2} (\overline{\nu}'_L \overline{\nu}'_R{}^c) M_\nu \begin{pmatrix} \nu'_L{}^c \\ \nu'_R{}^c \end{pmatrix} + H.c. \\
& + \dots,
\end{aligned} \tag{A.4}$$

where

$$M_\nu = \begin{pmatrix} 0 & m_{\nu D} \\ m_{\nu D}^T & M \end{pmatrix}, \tag{A.5}$$

V_{IL} and V_{IR} are 3 by 3 unitary mixing matrices for each species I , $m_u := vY_u/\sqrt{2}$, $m_d := vY_d/\sqrt{2}$, $m_e := vY_e/\sqrt{2}$ and $m_{\nu D} := vY_\nu/\sqrt{2}$. The final explicit term in (A.4) incorporates the see-saw mechanism via a 6 by 6 complex symmetric mass matrix. Since the elements in $m_{\nu D}$ are much less than those in M , one performs a rotation to obtain a 3 by 3 complex symmetric mass matrix for the *light* neutrinos. To a good approximation, these coincide with the left-handed weak eigenstates ν'_L , whereas three heavy neutrinos approximately correspond to the right-handed weak eigenstates ν'_R . The neutrino mass term of (A.4) becomes, to a good approximation,

$$-\mathcal{L}_\nu = \frac{1}{2} \overline{\nu}'_L{}^c m_\nu \nu'_L + \frac{1}{2} \overline{\nu}'_R{}^c M \nu'_R + H.c., \tag{A.6}$$

where $m_\nu := m_{\nu D}^T M^{-1} m_{\nu D}$ is a complex symmetric 3 by 3 matrix.

Choosing $V_{IL}^\dagger m_I V_{IR}$ to be diagonal, real and positive for $I \in \{u, d, e\}$, and $V_{\nu L}^T m_\nu V_{\nu L}$ to be diagonal, real and positive (all in increasing order of mass from the top left toward the bottom right of the matrix), we can identify the *non-primed mass* eigenstates

$$\begin{aligned}
\mathbf{u}_R &:= V_{uR}^\dagger \mathbf{u}'_R, & \mathbf{u}_L &:= V_{uL}^\dagger \mathbf{u}'_L, & \mathbf{d}_R &:= V_{dR}^\dagger \mathbf{d}'_R, \\
\mathbf{d}_L &:= V_{dL}^\dagger \mathbf{d}'_L, & \mathbf{e}_R &:= V_{eR}^\dagger \mathbf{e}'_R, & \mathbf{e}_L &:= V_{eL}^\dagger \mathbf{e}'_L. \\
\nu_L &:= V_{\nu L}^\dagger \nu'_L.
\end{aligned} \tag{A.7}$$

We may then find the CKM matrix V and the Pontecorvo-Maki-Nakagawa-Sakata (PMNS) matrix U in terms of the fermionic mixing matrices:

$$V = V_{uL}^\dagger V_{dL}, \quad U = V_{\nu L}^\dagger V_{eL}. \tag{A.8}$$

References

1. R. Aaij, et al., JHEP **08**, 055 (2017). DOI 10.1007/JHEP08(2017)055
2. R. Aaij, et al., Phys. Rev. Lett. **122**(19), 191801 (2019). DOI 10.1103/PhysRevLett.122.191801
3. M. Aaboud, et al., JHEP **04**, 098 (2019). DOI 10.1007/JHEP04(2019)098
4. S. Chatrchyan, et al., Phys. Rev. Lett. **111**, 101804 (2013). DOI 10.1103/PhysRevLett.111.101804
5. V. Khachatryan, et al., Nature **522**, 68 (2015). DOI 10.1038/nature14474
6. R. Aaij, et al., Phys. Rev. Lett. **118**(19), 191801 (2017). DOI 10.1103/PhysRevLett.118.191801
7. R. Aaij, et al., Phys. Rev. Lett. **111**, 191801 (2013). DOI 10.1103/PhysRevLett.111.191801
8. R. Aaij, et al., JHEP **02**, 104 (2016). DOI 10.1007/JHEP02(2016)104
9. M. Aaboud, et al., JHEP **10**, 047 (2018). DOI 10.1007/JHEP10(2018)047
10. A.M. Sirunyan, et al., Phys. Lett. B **781**, 517 (2018). DOI 10.1016/j.physletb.2018.04.030
11. V. Khachatryan, et al., Phys. Lett. **B753**, 424 (2016). DOI 10.1016/j.physletb.2015.12.020
12. C. Bobeth, M. Chrzaszcz, D. van Dyk, J. Virto, Eur. Phys. J. **C78**(6), 451 (2018). DOI 10.1140/epjc/s10052-018-5918-6
13. P.A. Zyla, et al., PTEP **2020**(8), 083C01 (2020). DOI 10.1093/ptep/ptaa104
14. M. Algueró, B. Capdevila, A. Crivellin, S. Descotes-Genon, P. Masjuan, J. Matias, M. Novoa Brunet, J. Virto, Eur. Phys. J. **C79**(8), 714 (2019). DOI 10.1140/epjc/s10052-019-7216-3, 10.1140/epjc/s10052-020-8018-3. [Addendum: Eur. Phys. J. C80, no.6, 511(2020)]
15. A.K. Alok, A. Dighe, S. Gangal, D. Kumar, JHEP **06**, 089 (2019). DOI 10.1007/JHEP06(2019)089
16. M. Ciuchini, A.M. Coutinho, M. Fedele, E. Franco, A. Paul, L. Silvestrini, M. Valli, Eur. Phys. J. **C79**(8), 719 (2019). DOI 10.1140/epjc/s10052-019-7210-9
17. J. Aebischer, W. Altmannshofer, D. Guadagnoli, M. Reboud, P. Stangl, D.M. Straub, Eur. Phys. J. **C80**(3), 252 (2020). DOI 10.1140/epjc/s10052-020-7817-x
18. A. Datta, J. Kumar, D. London, Phys. Lett. B **797**, 134858 (2019). DOI 10.1016/j.physletb.2019.134858
19. K. Kowalska, D. Kumar, E.M. Sessolo, Eur. Phys. J. **C79**(10), 840 (2019). DOI 10.1140/epjc/s10052-019-7330-2
20. A. Arbey, T. Hurth, F. Mahmoudi, D.M. Santos, S. Neshatpour, Phys. Rev. **D100**(1), 015045 (2019). DOI 10.1103/PhysRevD.100.015045
21. J. Ellis, M. Fairbairn, P. Tunney, Eur. Phys. J. **C78**(3), 238 (2018). DOI 10.1140/epjc/s10052-018-5725-0
22. B.C. Allanach, J. Davighi, S. Melville, JHEP **02**, 082 (2019). DOI 10.1007/JHEP08(2019)064, 10.1007/JHEP02(2019)082. [erratum: JHEP08,064(2019)]
23. R. Gauld, F. Goertz, U. Haisch, Phys. Rev. **D89**, 015005 (2014). DOI 10.1103/PhysRevD.89.015005
24. A.J. Buras, F. De Fazio, J. Girrbach, JHEP **02**, 112 (2014). DOI 10.1007/JHEP02(2014)112
25. A.J. Buras, J. Girrbach, JHEP **12**, 009 (2013). DOI 10.1007/JHEP12(2013)009
26. W. Altmannshofer, S. Gori, M. Pospelov, I. Yavin, Phys. Rev. **D89**, 095033 (2014). DOI 10.1103/PhysRevD.89.095033
27. A.J. Buras, F. De Fazio, J. Girrbach-Noe, JHEP **08**, 039 (2014). DOI 10.1007/JHEP08(2014)039
28. A. Crivellin, G. D'Ambrosio, J. Heeck, Phys. Rev. Lett. **114**, 151801 (2015). DOI 10.1103/PhysRevLett.114.151801

29. A. Crivellin, G. D'Ambrosio, J. Heeck, Phys. Rev. **D91**(7), 075006 (2015). DOI 10.1103/PhysRevD.91.075006
30. D. Aristizabal Sierra, F. Staub, A. Vicente, Phys. Rev. **D92**(1), 015001 (2015). DOI 10.1103/PhysRevD.92.015001
31. A. Crivellin, L. Hofer, J. Matias, U. Nierste, S. Pokorski, J. Rosiek, Phys. Rev. **D92**(5), 054013 (2015). DOI 10.1103/PhysRevD.92.054013
32. A. Celis, J. Fuentes-Martin, M. Jung, H. Serodio, Phys. Rev. **D92**(1), 015007 (2015). DOI 10.1103/PhysRevD.92.015007
33. A. Greljo, G. Isidori, D. Marzocca, JHEP **07**, 142 (2015). DOI 10.1007/JHEP07(2015)142
34. W. Altmannshofer, I. Yavin, Phys. Rev. **D92**(7), 075022 (2015). DOI 10.1103/PhysRevD.92.075022
35. B. Allanach, F.S. Queiroz, A. Strumia, S. Sun, Phys. Rev. **D93**(5), 055045 (2016). DOI 10.1103/PhysRevD.93.055045, 10.1103/PhysRevD.95.119902. [Erratum: Phys. Rev. **D95**, no. 11, 119902 (2017)]
36. A. Falkowski, M. Nardecchia, R. Ziegler, JHEP **11**, 173 (2015). DOI 10.1007/JHEP11(2015)173
37. C.W. Chiang, X.G. He, G. Valencia, Phys. Rev. **D93**(7), 074003 (2016). DOI 10.1103/PhysRevD.93.074003
38. D. Bečirević, O. Sumensari, R. Zukanovich Funchal, Eur. Phys. J. **C76**(3), 134 (2016). DOI 10.1140/epjc/s10052-016-3985-0
39. S.M. Boucenna, A. Celis, J. Fuentes-Martin, A. Vicente, J. Virto, Phys. Lett. **B760**, 214 (2016). DOI 10.1016/j.physletb.2016.06.067
40. S.M. Boucenna, A. Celis, J. Fuentes-Martin, A. Vicente, J. Virto, JHEP **12**, 059 (2016). DOI 10.1007/JHEP12(2016)059
41. P. Ko, Y. Omura, Y. Shigekami, C. Yu, Phys. Rev. **D95**(11), 115040 (2017). DOI 10.1103/PhysRevD.95.115040
42. R. Alonso, P. Cox, C. Han, T.T. Yanagida, Phys. Rev. **D96**(7), 071701 (2017). DOI 10.1103/PhysRevD.96.071701
43. R. Alonso, P. Cox, C. Han, T.T. Yanagida, Phys. Lett. **B774**, 643 (2017). DOI 10.1016/j.physletb.2017.10.027
44. Y. Tang, Y.L. Wu, Chinese Physics C **42**(3), 033104 (2018). URL <http://stacks.iop.org/1674-1137/42/i=3/a=033104>
45. C. Bonilla, T. Modak, R. Srivastava, J.W.F. Valle, Phys. Rev. **D98**(9), 095002 (2018). DOI 10.1103/PhysRevD.98.095002
46. D. Bhatia, S. Chakraborty, A. Dighe, JHEP **03**, 117 (2017). DOI 10.1007/JHEP03(2017)117
47. C.H. Chen, T. Nomura, Physics Letters B **777**, 420 (2018). DOI <https://doi.org/10.1016/j.physletb.2017.12.062>. URL <http://www.sciencedirect.com/science/article/pii/S0370269318300029>
48. G. Faisel, J. Tandeau, JHEP **02**, 074 (2018). DOI 10.1007/JHEP02(2018)074
49. K. Fuyuto, H.L. Li, J.H. Yu, Phys. Rev. D **97**, 115003 (2018). DOI 10.1103/PhysRevD.97.115003. URL <https://link.aps.org/doi/10.1103/PhysRevD.97.115003>
50. L. Bian, H.M. Lee, C.B. Park, Eur. Phys. J. **C78**(4), 306 (2018). DOI 10.1140/epjc/s10052-018-5777-1
51. M. Abdullah, M. Dalchenko, B. Dutta, R. Eusebi, P. Huang, T. Kamon, D. Rathjens, A. Thompson, Phys. Rev. D **97**, 075035 (2018). DOI 10.1103/PhysRevD.97.075035. URL <https://link.aps.org/doi/10.1103/PhysRevD.97.075035>
52. S.F. King, JHEP **09**, 069 (2018). DOI 10.1007/JHEP09(2018)069
53. G.H. Duan, X. Fan, M. Frank, C. Han, J.M. Yang, Phys. Lett. **B789**, 54 (2019). DOI 10.1016/j.physletb.2018.12.005
54. B.C. Allanach, J. Davighi, JHEP **12**, 075 (2018). DOI 10.1007/JHEP12(2018)075
55. B.C. Allanach, T. Corbett, M.J. Dolan, T. You, JHEP **03**, 137 (2019). DOI 10.1007/JHEP03(2019)137
56. Z. Kang, Y. Shigekami, JHEP **11**, 049 (2019). DOI 10.1007/JHEP11(2019)049
57. L. Calibbi, A. Crivellin, F. Kirk, C.A. Manzari, L. Vernazza, Phys. Rev. D **101**(9), 095003 (2020). DOI 10.1103/PhysRevD.101.095003
58. B. Capdevila, A. Crivellin, C.A. Manzari, M. Montull, (2020)
59. J. Davighi, M. Kirk, M. Nardecchia, (2020)
60. A. Crivellin, J. Fuentes-Martin, A. Greljo, G. Isidori, Phys. Lett. **B766**, 77 (2017). DOI 10.1016/j.physletb.2016.12.057
61. J.F. Kamenik, Y. Soreq, J. Zupan, Phys. Rev. **D97**(3), 035002 (2018). DOI 10.1103/PhysRevD.97.035002
62. J.E. Camargo-Molina, A. Celis, D.A. Faroughy, Phys. Lett. **B784**, 284 (2018). DOI 10.1016/j.physletb.2018.07.051
63. D. Borah, L. Mukherjee, S. Nandi, (2020)
64. C.D. Froggatt, H.B. Nielsen, Nucl. Phys. **B147**, 277 (1979). DOI 10.1016/0550-3213(79)90316-X
65. F. Englert, R. Brout, Phys. Rev. Lett. **13**, 321 (1964). DOI 10.1103/PhysRevLett.13.321. URL <https://link.aps.org/doi/10.1103/PhysRevLett.13.321>
66. P.W. Higgs, Phys. Rev. Lett. **13**, 508 (1964). DOI 10.1103/PhysRevLett.13.508. URL <https://link.aps.org/doi/10.1103/PhysRevLett.13.508>
67. Y. Amhis, et al., Eur. Phys. J. **C77**(12), 895 (2017). DOI 10.1140/epjc/s10052-017-5058-4
68. D. King, A. Lenz, T. Rauh, JHEP **05**, 034 (2019). DOI 10.1007/JHEP05(2019)034
69. B.C. Allanach, J.M. Butterworth, T. Corbett, JHEP **08**, 106 (2019). DOI 10.1007/JHEP08(2019)106
70. S.R. Mishra, et al., Phys. Rev. Lett. **66**, 3117 (1991). DOI 10.1103/PhysRevLett.66.3117. URL <https://link.aps.org/doi/10.1103/PhysRevLett.66.3117>
71. M. Pospelov, Phys. Rev. D **80**, 095002 (2009). DOI 10.1103/PhysRevD.80.095002
72. A.M. Sirunyan, et al., Phys. Lett. B **792**, 345 (2019). DOI 10.1016/j.physletb.2019.01.072
73. J. Alwall, R. Frederix, S. Frixione, V. Hirschi, F. Maltoni, O. Mattelaer, H.S. Shao, T. Stelzer, P. Torrielli, M. Zaro, JHEP **07**, 079 (2014). DOI 10.1007/JHEP07(2014)079
74. M. Aaboud, et al., Eur. Phys. J. **C78**(7), 565 (2018). DOI 10.1140/epjc/s10052-018-5995-6
75. M. Aaboud, et al., Phys. Rev. **D99**(9), 092004 (2019). DOI 10.1103/PhysRevD.99.092004
76. G. Aad, et al., JHEP **07**, 157 (2015). DOI 10.1007/JHEP07(2015)157
77. G. Aad, et al., Phys. Lett. **B796**, 68 (2019). DOI 10.1016/j.physletb.2019.07.016
78. G. Aad, et al. Search for high-mass dilepton resonances using 139 fb⁻¹ of pp collision data collected at $\sqrt{s} = 13$ TeV with the ATLAS detector (2019). DOI <https://doi.org/10.17182/hepdata.88425>. <https://www.hepdata.net/record/88425>
79. C. Degrande, C. Duhr, B. Fuks, D. Grellscheid, O. Mattelaer, T. Reiter, Comput. Phys. Commun. **183**, 1201 (2012). DOI 10.1016/j.cpc.2012.01.022
80. A. Alloul, N.D. Christensen, C. Degrande, C. Duhr, B. Fuks, Comput. Phys. Commun. **185**, 2250 (2014). DOI 10.1016/j.cpc.2014.04.012

81. M. Lim, F. Maltoni, G. Ridolfi, M. Ubiali, *JHEP* **09**, 132 (2016). DOI 10.1007/JHEP09(2016)132
82. M. Aaboud, et al., *JHEP* **10**, 182 (2017). DOI 10.1007/JHEP10(2017)182
83. B. Allanach, J. Davighi, *Eur. Phys. J. C* **79**(11), 908 (2019). DOI 10.1140/epjc/s10052-019-7414-z
84. J. Davighi, Topological effects in particle physics phenomenology. Ph.D. thesis, Cambridge U. (main) (2020). DOI 10.17863/CAM.47560